Stabilization of ZnO quantum dots by preferred 1:2 interaction with a liquid crystal molecule

Wallison C. Costa [a], Crislaine Sandri [b], Samara de Quadros [c], Ana L.E.P. Silva [c], Juliana Eccher [a], Lizandra M. Zimmermann [c,*], Jose R. Mora [d], Harald Bock [e], Ivan H. Bechtold [a,*]

[a] Departamento de Física, Universidade Federal de Santa Catarina, Florianópolis 88040-900, SC, Brazil
[b] Departamento de Química, Universidade Federal de Santa Catarina, Florianópolis 88040-900, SC, Brazil
[c] Departamento de Química, Universidade Regional de Blumenau, CP 1507, Blumenau 89030-903, SC, Brazil
[d] Universidad San Francisco de Quito, Departamento de Ingeniería Química, Diego de Robles y Vialnteroceánica, Quito 17-1200-841, Ecuador
[e] Centre de Recherche Paul Pascal, Université de Bordeaux & CNRS, 115 Avenue Schweitzer, 33600 Pessac, France

ARTICLE INFO

Article history:
Received 9 January 2020
Received in revised form 3 April 2020
Accepted 1 May 2020
Available online 04 May 2020

ABSTRACT

Zinc oxide (ZnO) quantum dots were synthesized in the presence of a columnar liquid crystalline perylene derivative. The liquid crystal molecules did not influence the nanoparticles' growth, and surprisingly they were efficient in stabilizing the colloidal dispersion over several months. For the first time, the quantity of ZnO units present in the ~4 nm sized ZnO nanoparticles was determined from the supramolecular interaction between the nanoparticles and the liquid crystal molecules as well as by analyzing the stoichiometry of the mixture. The quantity of ZnO units was also confirmed by theoretical studies performed by means of DFT calculations. The mixture was efficiently applied for methylene blue photodegradation.

1. Introduction

The bulk phase of zinc oxide (ZnO) has a band gap of 3.37 eV, and its exciton binding energy is 60 mV at room temperature. This material absorbs light in the UV region (200–375 nm) and emits close to 520 nm as a result of structural defects such as zinc and oxygen vacancies, or due to surface impurities [1–3]. Bulk ZnO is an n-type semiconductor [4] with excellent mechanical and thermal stability that can have the crystalline structures of hexagonal wurtzite, zinc blende and rock salt, in which bonding is characterized by a tetrahedral geometry and sp^3 hybridization [5–7].

Quantum dots (QDs) are semiconducting nanomaterials with diameters ranging from 2 to 10 nm and three-dimensional (3D) quantum confinement effects that lead to distinct optical and electronic properties [8]. ZnO QDs have received special attention due to their low toxicity and have found many applications in light emitting devices [9,10], electrochemical sensors [11,12], biological markers [13,14] and photocatalysis [15,16]. Visible fluorescence emission ranging from blue to yellow under ultraviolet (UV) light excitation can be obtained by controlling the nanoparticles' diameter [1] and their structural defects [3].

As a photocatalyst, ZnO QDs have already been used under excitation by natural and artificial UV and visible light in their pure form or combined with other materials for the degradation of various potentially toxic molecules [17,18]. Associating the photocatalytic activity of ZnO with QD nanostructures is lucrative, as decreasing semiconductor size increases surface area, allows abundant surface states in various morphologies and opens new possibilities for device design [19,20].

Molecular systems with complementary energy levels have been investigated in conjunction to enlarge the visible light absorption for photovoltaic applications, where the stability of the combined system, especially under light irradiation, is essential for long lifetimes of the devices. Liquid crystals (LCs) combine molecular order and fluidity, and they have been used for many technological applications, in displays [21], in organic electronic devices such as OLEDs [22], OFETs [23] and OSCs [24], and in nanocomposite systems with metallic nanoparticles [25], carbon nanotubes [26] and quantum dots [27] in order to improve the electro-optical properties of the combined systems [24,28,29]. Liquid crystalline perylene derivatives absorb and emit visible light, form long-range ordered π-aggregates in columnar superstructures and show high electron mobility with pronounced n-type semiconducting character [30]. We previously demonstrated that OLED performance was improved by mixing two perylene derivatives compared to the individual materials alone [31].

In the present work, ZnO QDs were synthesized in the presence of a LC perylene derivative to combine two n-type semiconductors and to increase absorption range, but with superimposed photoluminescence.

* Corresponding authors.
E-mail addresses: lmz@furb.br (L.M. Zimmermann), ivan.bechtold@ufsc.br (I.H. Bechtold).

The presence of the perylene did not affect the ZnO nanoparticle growth, and it proved to be efficient in the stabilization of the ZnO QD colloidal dispersions, despite the strong tendency of nanoparticles to aggregate in a bulk liquid crystal host [32]. The experimental determination of supramolecular interactions supplemented by theoretical modeling allowed the determination of the number of ZnO units in the ZnO nanoparticles. The prepared ethanolic dispersion demonstrated that ZnO was selective for photodegradation of methylene blue, with no photochemical degradation effect on the perylene derivative.

2. Materials and methods

2.1. Materials

Commercial zinc acetate dihydrate ($Zn(CH_3COO)_2 \cdot 2H_2O$) ACS ° 99% (Sigma-Aldrich), sodium hydroxide (NaOH) ACS reagent ≥ 99.38% (Vetec), and ethanol P.A. ACS 99.5% (Sigma-Aldrich) was used as received. A 100 mL three-necked round bottom glass flask was used as a reactor. A hot plate with magnetic stirrer was used to control temperature and to homogenize the reaction.

The synthesis and characterization of the perylene based liquid crystalline material, 3,9(10)-bis-(2-methoxyethoxycarbonyl)-4,10(9)-bis (2-(2-methoxyethoxy)ethoxycarbonyl)perylene (PerLC), was published elsewhere [31,33]. The molecule (inset of Fig. 2) has a disc-like structure with diameter 16.3 Å determined by X-ray diffraction and presents a stable hexagonal columnar mesomorphism from room temperature until 150 °C.

2.2. Synthesis of colloidal ZnO QDs

QDs were synthesized using the sol-gel method, based on methodologies reported in the literature [34–37] choosing ethanol as solvent [37,38]. Initially stock solutions of NaOH and $Zn(CH_3COO)_2 \cdot 2H_2O$ were prepared. Approximately 0.01 g of each reagent were weighted and dissolved in 10 mL of ethanol, and the solutions were homogenized at 60 °C in a water bath with stirring. Then, the volume of each reagent to be added to the reactor was determined to obtain a total volume of 15 mL of reaction at 2.0×10^{-3} mol L^{-1} of $Zn(CH_3COO)_2 \cdot 2H_2O$ and 2.5×10^{-3} mol L^{-1} of NaOH. The appropriate volume of ethanol was added to the reactor to complete the final volume. The stock solutions and the reactor are then placed in an ice bath (0 °C), followed by the addition of the calculated volume of the stock solution of $Zn(CH_3COO)_2 \cdot 2H_2O$ and the system was maintained under agitation for 10 min for homogenization. To produce the QDs, the predetermined volume of NaOH was added dropwise, and the timer is set after the first drop. One min later, the reactor is transferred from the ice bath to a water bath at 60 °C and is stirred at that temperature for 120 min, when the reaction is finished by taking the reactor out of the water bath and stopping stirring.

For the synthesis of ZnO-PerLC QDs a stock solution of PerLC was prepared at the concentration of 8.7×10^{-4} mol L^{-1} and 343 μL of this solution was added after the addition of zinc acetate to the three-neck round bottom glass flask to obtain a concentration of 2.0×10^{-5} mol L^{-1}, and the system was maintained under constant stirring for 10 min.

In order to investigate the effect of the concentration of PerLC over the ZnO QDs dispersion, a stock solution of PerLC at 1.0 mg mL^{-1} (1.3×10^{-3} mol L^{-1}) was prepared and added to the colloidal dispersion of ZnO, at the beginning of the reaction, to obtain three different PerLC concentrations (1.0×10^{-4} mol L^{-1}, 1.0×10^{-5} mol L^{-1} and 1.0×10^{-6} mol L^{-1}).

2.3. ZnO-doped perylene LC solid

ZnO QDs in colloidal dispersion were prepared as described in Section 2.2. An aliquot of 3.3 mL of the synthesis was separated to yield 0.53 mg of ZnO QDs and then 9.47 mg of PerLC was dissolved in that volume in order to achieve 5.3% and 94.7% of ZnO and PerLC, respectively. The mixture was homogenized in an ultrasound bath for 15 min. To obtain the solid, the solvent was evaporated keeping the mixture in an oven at 60 °C for 24 h.

2.4. Characterization

The UV–Vis absorbance spectra of ZnO QDs and PerLC dissolved in ethanol were collected with an Ocean Optics USB4000 spectrophotometer. For the photoluminescence (PL) measurements a Hitachi fluorescence spectrophotometer (Model F-7000) was used.

The shape and size of the nanoparticles were determined by transmission electron microscopy (TEM) using a JEOL JEM-2100 microscope operating at 200 kV.

The hydrodynamic diameter of ZnO and ZnO-PerLC nanoparticles was obtained using Malvern's ZetaSizer Nano S equipment. This analysis was performed after 2 h, 1 day and 14 days after the synthesis.

Optical textures of the materials sandwiched between two glass slides were obtained using an Olympus BX50 polarizing optical microscope (POM) equipped with a Mettler Toledo FP-82 hot stage to control the temperature.

2.5. Supramolecular interaction of ZnO QDs with perylene derivative

A 1.0×10^{-4} mol L^{-1} solution of PerLC was prepared in ethanol. ZnO QDs were added (ZnO unities = 2.0×10^{-3} mol L^{-1}) to the titrant in order to maintain constant its concentration during PerLC additions. 2.0 mL of colloidal dispersion of ZnO QDs into a 3 mL quartz-cuvette was titrated by successive additions of 20 μL of the PerLC solution. After each addition, absorbance spectra were collected using a Shimadzu UV-1800 spectrophotometer.

2.6. Photodegradation of methylene blue with ZnO QDs with and without perylene derivative

Photocatalysis essays were performed using a 5.0 mL volumetric flask as reactor. This flask was placed in a water reflux system in order to remain at room temperature (23–25 °C) under constant magnetic stirring. To the flask was added 100 μL of a 1.0×10^{-3} mol L^{-1} stock solution of methylene blue (MB) in order to get 2.0×10^{-5} mol L^{-1} in the colloidal dispersion of ZnO QDs (2.0×10^{-3} mol L^{-1} ZnO, without or with 2.0×10^{-5} mol L^{-1} PerLC). The reaction system was sunlight-irradiated for two hours between 11 a.m. and 02 p.m. (period of highest light intensity), using a glass to filter the radiation and on cloudless days, keeping the same conditions for all photocatalysis essays. Aliquots of the system under irradiation were taken and analyzed by scanning absorbance from 200 to 700 nm on a Shimadzu UV-1800 spectrophotometer after 0, 5, 10, 20, 30, 40, 50, 60, 90 and 120 min. The kinetics of the photodegradation was analyzed by using Eq. (1).

$$A_t = A_0 e^{(-k_{app} t)} \quad (1)$$

where A_t is the absorbance at the maximum absorbance wavelength of MB (655 nm) at each time, t; A_0 is the initial absorbance, and k_{app} is the apparent first-order constant.

3. Results and discussion

Fig. 1 shows the absorbance spectra obtained over the temporal evolution of the colloidal dispersion of ZnO QDs in ethanol at room temperature, after the 2 h reaction was stopped. In a previous work, the experimental conditions using this synthetic procedure were determined using 2-propanol, where without stabilizer the ZnO nanoparticles grew up to the limit of the associated energy value of bulk ZnO (3.37 eV) with 120 min of reaction [34]. Here, using ethanol and without

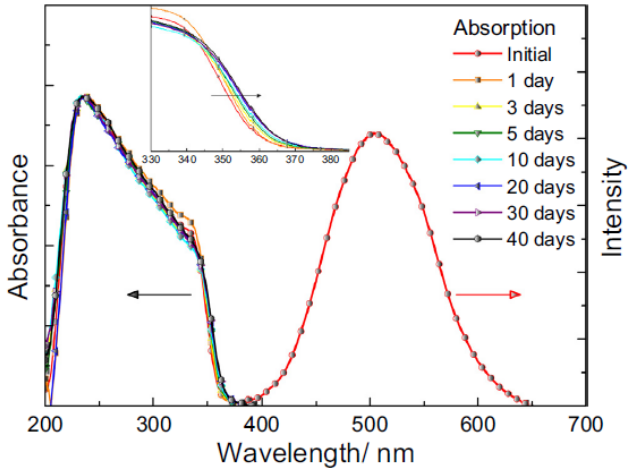

Fig. 1. Absorption time evolution of ZnO QDs (2.0×10^{-3} mol L^{-1} ZnO) without stabilizer during 40 days, and PL spectrum immediately after quantum dot formation. Excitation wavelength $\lambda_{exc} = 335$ nm.

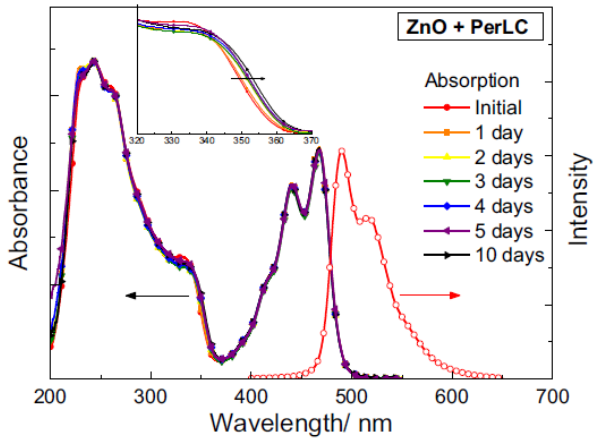

Fig. 3. Absorption time evolution of ZnO QDs (ZnO = 2.0×10^{-3} mol L^{-1}) + PerLC (1.0×10^{-4} mol L^{-1}) without stabilizer during 10 days, where the reaction was stopped after 120 min. PL spectrum after 120 min of reaction. Excitation wavelength $\lambda_{exc} = 335$ nm.

stabilizer, a slight displacement of the absorption spectrum toward longer wavelengths is observed over 40 days. The optical band gap was determined by Tauc plot based on UV–Vis absorption, being 3.50 eV and 3.45 eV for 120 min and 40 days, respectively. These values confirm that, just after the synthesis, the ZnO nanocrystals are in the quantum confinement regime. If the onset of ZnO absorption band is ≥370 nm, the band gap energy corresponds to the bulk phase [39]. The initial PL spectrum is in the range 400–650 nm (Fig. 1), with a maximum around 505 nm, which is typical for ZnO QD emission.

Fig. 2 shows the absorption and PL (with excitation at 467 nm) of PerLC in ethanol at a concentration of 1.0×10^{-5} mol L^{-1}. The vibronic absorption and PL bands are typical for perylene based molecules. In conjunction with the ZnO QDs, PerLC offers an additional absorption band at 380–500 nm, which increases light absorption of the composite system. Notwithstanding this, the PL of both is in the same spectral region, being broader for ZnO.

The absorption and emission spectra of the ZnO QDs synthesized in the presence of PerLC (1.0×10^{-4} mol L^{-1}) are presented in Fig. 3, where the concentration of ZnO units 2.0×10^{-3} mol L^{-1}. The absorption is the sum of the individual components, while the PL is dominated by the PerLC emission profile, even when excited within long-wavelength end of the absorption band of ZnO at 335 nm, where the absorption of PerLC is very low. The intensity of PerLC PL when excited in the ZnO absorption region (335 nm) is around one order of magnitude weaker than when excited at the maximum absorption of PerLC (467 nm). Absolute PL quantum yields were obtained to be 84% for PerLC ($\lambda_{ex} = 467$ nm) and 15% for ZnO QDs ($\lambda_{ex} = 350$ nm).

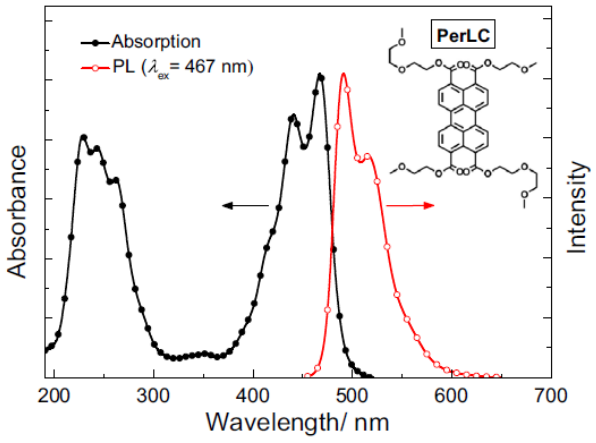

Fig. 2. Absorption and PL spectra of the LC perylene derivative in ethanol at concentrations of 1.0×10^{-4} mol L^{-1}. Inset: molecular structure (only one of two regio-isomers is sketched). Molar mass = 749.06 g/mol.

The time evolution during 10 days shows the same absorption characteristics, where the onset is the same as in case of pure ZnO QDs, indicating that the nanoparticle growth is not affected by the presence of the PerLC molecules during the reaction. The same was observed for a PerLC concentration of 1.0×10^{-5} mol L^{-1}, see Fig. S1.

Fig. 4 shows TEM images of ZnO QDs synthetized without (a, b) and with (c, d) the presence of PerLC, where the measured particles diameter is 4.1 ± 0.5 nm and 4.0 ± 0.4 nm, respectively, with size dispersion around 10%. High resolution TEM images of both cases are shown in Fig. 4(b) and (d), where interplanar spacings of 0.28 nm and 0.26 nm were obtained, corresponding to the planes (100) and (002), respectively. This crystalline structure is compatible with the ZnO wurtzite hexagonal phase according to the ICSD 34477 crystallographic card [40]. These results show that the presence of PerLC during the synthesis does not affect the particle size and crystallographic structure.

Fig. 5 shows pictures of the colloidal dispersions under UV light excitation at 365 nm. After 60 days, the dispersion without PerLC precipitates at the bottom of the vessel, being evident from the yellow PL under UV illumination, Fig. 5(C). On the other hand, Fig. 5(A) and (B) shows that with PerLC concentrations of 1.0×10^{-4} mol L^{-1} and 1.0×10^{-5} mol L^{-1}, respectively, the dispersion is stable. Surprisingly, the PerLC molecules act as stabilizer for the ZnO QDs colloidal dispersions [32]. The dispersion samples of Fig. 5 are identical with those of Figs. 1, 3 and S2, photographed after 1 year of storage at room temperature. Fig. 5(D) shows the sample of Fig. 5(C) after sonicating for 5 min.

The hydrodynamic diameter of the colloidal dispersions (ZnO QDs and ZnO QDs + PerLC) was measured by dynamic light scattering (DLS) as a function of time (Fig. S2). Just after the synthesis the hydrodynamic diameter of the ZnO QDs is smaller than for ZnO QDs prepared in the presence of PerLC. The onsets of the absorbance spectra and the TEM measurements both indicate that the size of the QDs themselves is not affected by the presence of PerLC during the synthesis. Therefore, the about 5 nm larger hydrodynamic sphere must result from the adsorption of PerLC molecules onto the QD surfaces. One day after stopping reaction the hydrodynamic diameter increased 92.5% and 27.3% for pure ZnO QDs and ZnO QDs + PerLC, respectively, which can be associated to QD aggregation. The role of the presence of PerLC on the colloidal ZnO QD dispersion is even more striking after longer periods: after 21 days the hydrodynamic diameter has increased to 808% and 373% without and with PerLC, respectively. Taking the DLS

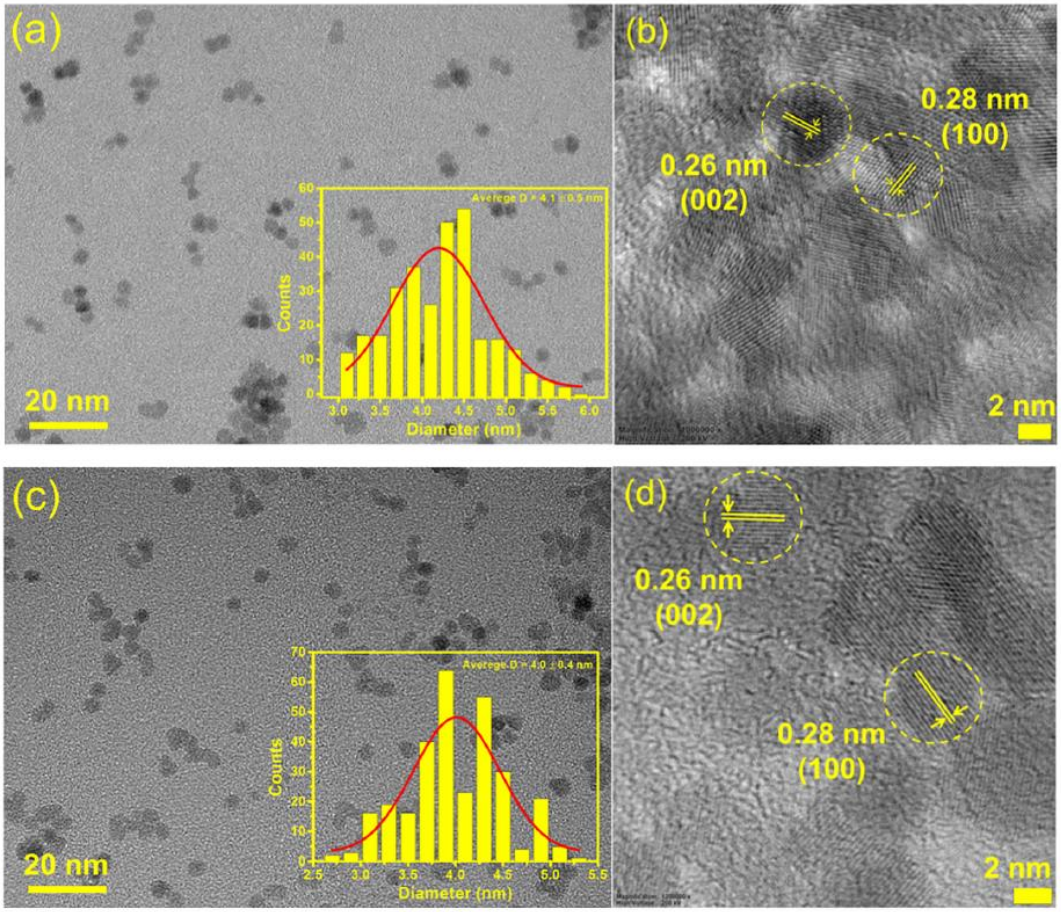

Fig. 4. TEM images and size distribution histograms (insets) of ZnO QDs (ZnO = 2.0×10^{-3} mol L^{-1}) synthesized without (a, b) and with (c, d) presence of PerLC (2.0×10^{-5} mol L^{-1}). High resolution TEM images (b) and (d) show the particles' crystalline periodicities.

measurements of the samples shown in Fig. 5, the polydispersity index was very high (100%) indicating the continuous formation of aggregates (results not presented). Thus, the presence of PerLC, lowers the size aggregates, prevents the colloidal system from precipitate, despite not preventing the aggregate growth.

In order to investigate the supramolecular interaction of the PerLC molecules with the ZnO QDs, the spectral absorption changes of the ZnO QDs in the UV–vis region were studied by adding PerLC solutions, see Fig. 6(A). With the first addition of PerLC at concentration of 9.90×10^{-7} mol L^{-1} a decrease in the ZnO absorbance at 345 nm was

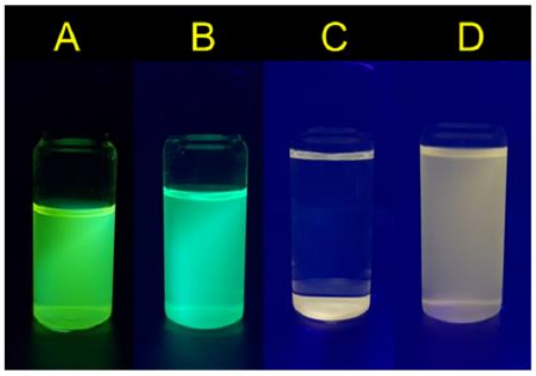

Fig. 5. Photographs of colloidal dispersions of ZnO QDs after 1 year of storage; (A) and (B): with addition of PerLC during the reaction (A: 1.0×10^{-4} mol L^{-1}; B: 1.0×10^{-5} mol L^{-1}); (C): pure ZnO QDs without PerLC. λ_{exc} = 365 nm. The concentration of ZnO is 2.0×10^{-3} mol L^{-1} in all dispersions. (D) shows sample (C) after sonicating for 5 min.

observed, which is associated to the first interactions between both chemical species [41,42]. Subsequently, as the PerLC concentration increases, the absorbance at 468 nm increases up following two linear tendencies (Fig. 6(B)). Taking those data and treating them considering a supramolecular complex formation, the mole ratio method was used in order to obtain the stoichiometry of the complex. This method was elaborated by Beltrán-Porter et al. [43] and Ackermann &Connors [44] that assign a measurable property of the system where the substrate (here ZnO) concentration is held constant and the ligand (here PerLC) concentration is varied. The plot with the measurable property against the ligand/substrate ratio should show a discontinuity or an abrupt change where the stoichiometric ratio can be found.

The stoichiometric ratio between PerLC and ZnO was determined in triplicate experiments and found to be (2.0 ± 0.1):1000 from the intersection of the two trend lines in Fig. 6(B), obtained by extrapolating independent linear fittings over the two data sets (with $R^2 > 0.99$), before and after the intersection point. This demonstrates that the Beltrán-Porter approach can conveniently be used to obtain adsorbate/particle ratios from absorption spectra of the molecular component on titration, also to estimate the number of ZnO units per particle, once 1000 is very close 972, determined theoretically to be the number of ZnO units per ZnO QD particle (see below).

In support, theoretical studies were performed by means of DFT calculations. The **hseh1pbe** functional was employed and as basis set the pseudo potential **lanl2dz** [quantum mechanics level (QM)]. The force field UFF was employed for the molecular mechanic (MM) level of theory. The **hseh1pbe** functional has been widely used for the study of crystalline surfaces of metal oxides [44,45]. In a first stage, the wurtzite structure of the primitive cell of ZnO was optimized at the QM level by

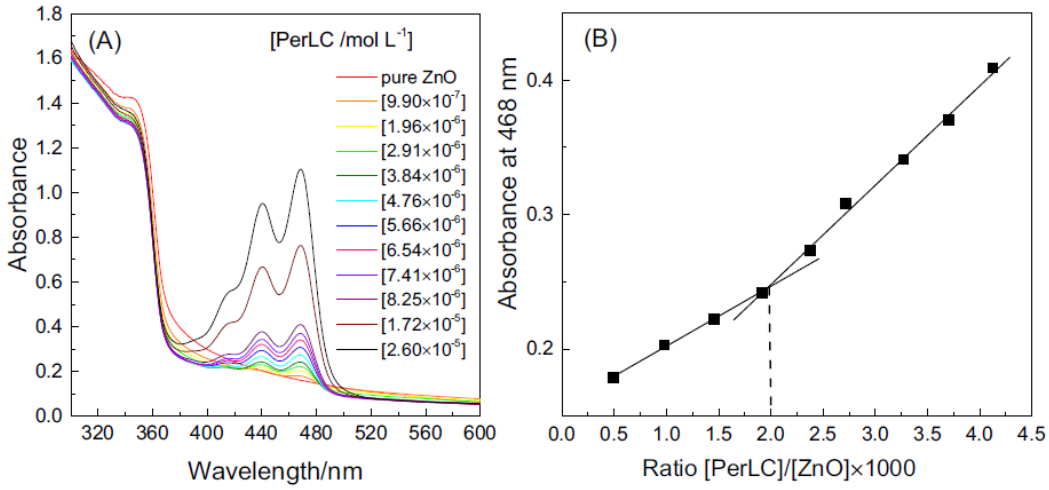

Fig. 6. (A) UV–vis spectra of colloidal dispersion of ZnO QDs with increasing amounts of PerLC. (B) Absorbance values at 468 nm as a function of the molar ratio between PerLC and ZnO concentrations by increasing additions of titrant (PerLC).

using the crystal 17 software [46,47] and the expansion of the cell was performed until the achievement of a symmetric structure of 972 units of ZnO, and as result was obtained an particle of a diameter of 4.69 nm, which is in good agreement with the experimental results of Fig. 4 (≈4 nm). 972 ZnO units constituting a QD closely coincide with the 2:926 ratio obtained above, indicating that 1 QD is surrounded by 2 PerLC molecules. The optimized QD structure is shown in Fig. 7. For the first time, the results here shown (combining the Beltrán-Porter approach and the theoretical studies) support that the number of ZnO units per particle can be obtained from the particle size.

With respect to the interaction of PerLC with the surface of the nanoparticle, three possible planes of interactions were considered for the estimation of the binding energy: the plane 100 with the oxygen atoms exposed (O-ZnO-100), the plane 100 with the Zn atoms exposed (Zn-ZnO-100) and the plane Zn-O (see Fig. 8(A)). The plane 100 was selected because it was well characterized by the TEM analysis (Fig. 4) and it is also commonly used in the literature [48,49].

For the interaction energy calculation of PerLC with the ZnO surface, a QM/MM calculation was performed for each plane separately and the PerLC was considered in the QM level, while the surface was considered in the MM level. These calculations were performed by using the software Gaussian 16 [50]. The atoms positions of the ZnO particle were fixed in order to maintain the previous optimized structure. Then, the binding energy (BE) [51,52] can be estimated by Eq. (2) below:

$$BE = E_{PerLC-surface} - (E_{surface} + E_{PerLC}) \quad (2)$$

where E is the electronic energy and surface represent the three evaluated surfaces (O-ZnO-100, Zn-ZnO-100 and Zn-O). In Fig. 8(B), the interaction for each plane and the corresponding binding energies were found for the three cases, with the most favorable interaction with the Zn-ZnO-100 plane (−1.59 eV), suggesting a relatively strong interaction between ZnO and PerLC, which can impede ZnO QDs aggregation and be responsible for the colloidal stabilization over time upon PerLC addition.

The ZnO efficiency as photocatalyzer for MB degradation under sunlight irradiation was investigated both for pure ZnO nanoparticles and those made in the presence of PerLC (2.0×10^{-5} mol L^{-1}) (Fig. 9).

The photodegradation of MB using ZnO QDs without and with PerLC were similar. In both cases, the absorption bands of the MB (655 nm) disappeared after 2 h irradiation (see Fig. S3). The rate constants from Eq. (1) were very similar, with $k_{app} = 0.19 \pm 0.025$ min^{-1} for pure ZnO and $k_{app} = 0.18 \pm 0.019$ min^{-1} for ZnO + PerLC. This indicates that the presence of PerLC does not hinder the photocatalytic effect of

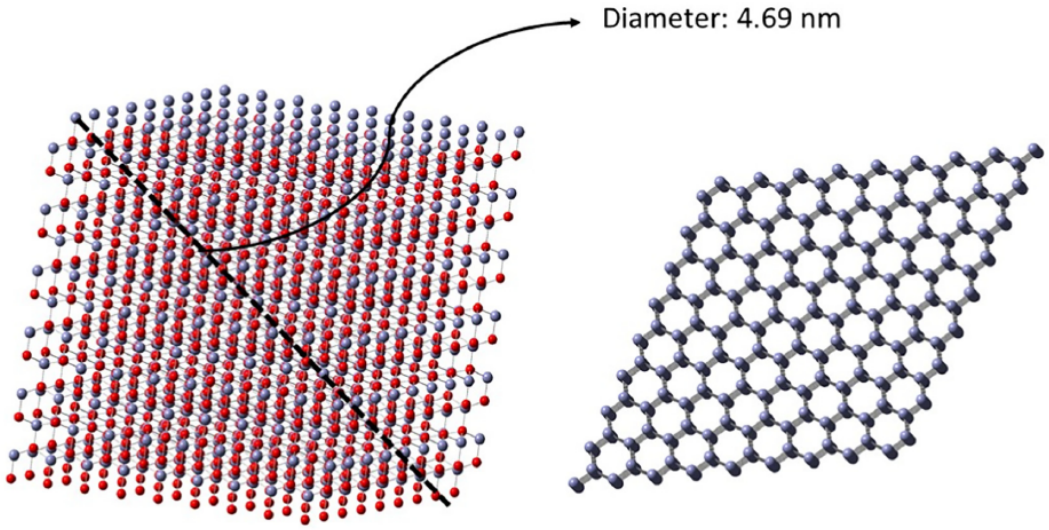

Fig. 7. Optimized structure of a nanoparticle of 972 units of ZnO.

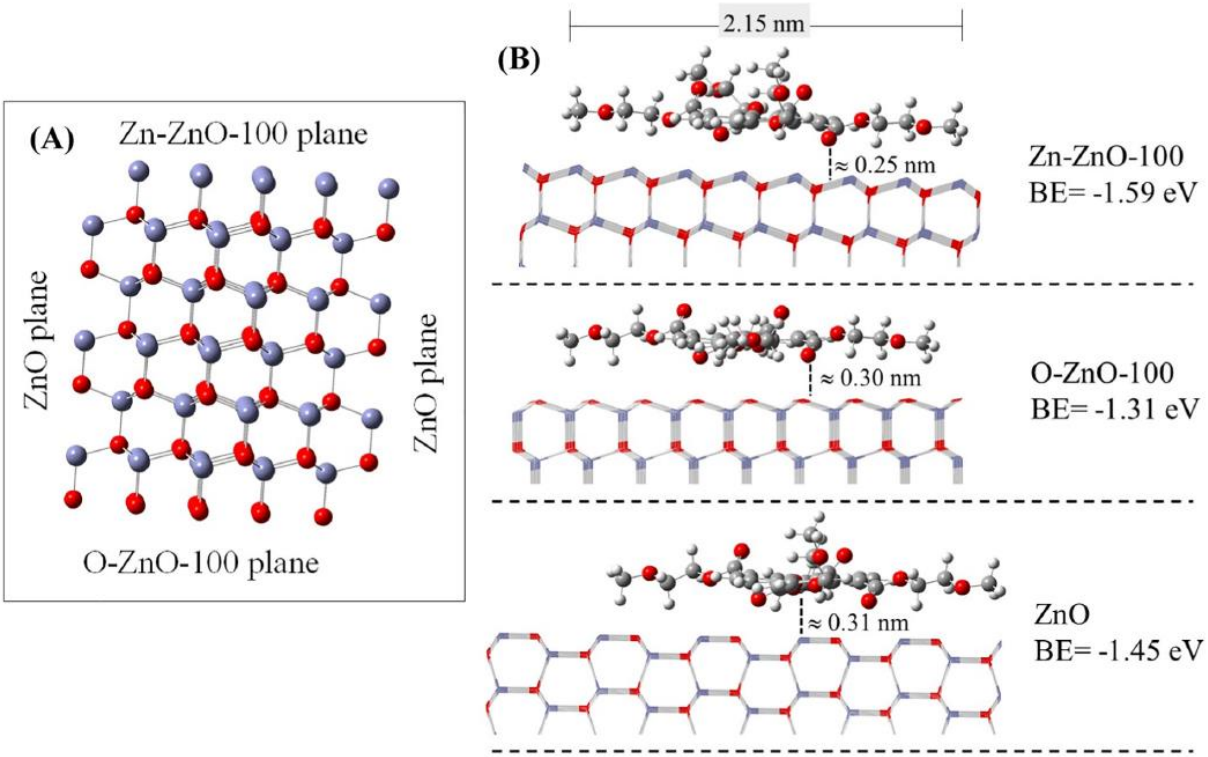

Fig. 8. (A) Possible planes for the PerLC interaction with the surfaces of ZnO QDs and (B) the binding energy for the three possible planes.

ZnO on MB. Fig. 9(B) shows the selectivity of ZnO QDs in the promotion of MB photodegradation, since only the absorption bands of MB decrease, while the absorption bands of PerLC are not affected.

In view of the strong coupling between the ZnO QDs and the PerLC molecules we also investigated the doping of the PerLC columnar LC matrix with ZnO QDs (5.3 wt%). Optical textures were captured with polarized light optical microscopy (POM) during cooling from the isotropic phase (157 °C) to room temperature. Fig. 10 shows the recorded images of pure PerLC (on the top) and doped with ZnO QDs (on the bottom) at temperatures of 155 °C (a, d), 135 °C (b, e) and 25 °C (c, f), for a cooling rate of 5 °C min^{-1}.

Images at 155 °C show that pure PerLC has already entered the Col_h mesophase, while the ZnO-doped PerLC is still in the isotropic phase, indicating that ZnO QDs are incorporated in the hexagonal columnar lattice of PerLC, decreasing the isotropic-Col_h transition temperature. For the doped sample the isotropic-Col_h transition starts around 140 °C (Fig. 10(e)). This concords with reports on the reduction of transition temperatures by doping columnar LCs with metallic nanoparticles [25]. The texture of the doped sample exhibits smaller domains (Fig. 10(e, f)) compared to pure PerLC, which shows that the QDs disrupt the macroscopic homogeneity of the LC without, however, destroying the microscopic and mesoscopic Col_h organization. For the pure and doped samples the images obtained at 25 °C (Fig. 10(c, f)) indicate that the Col_h mesophase is preserved at room temperature and no crystallization was observed.

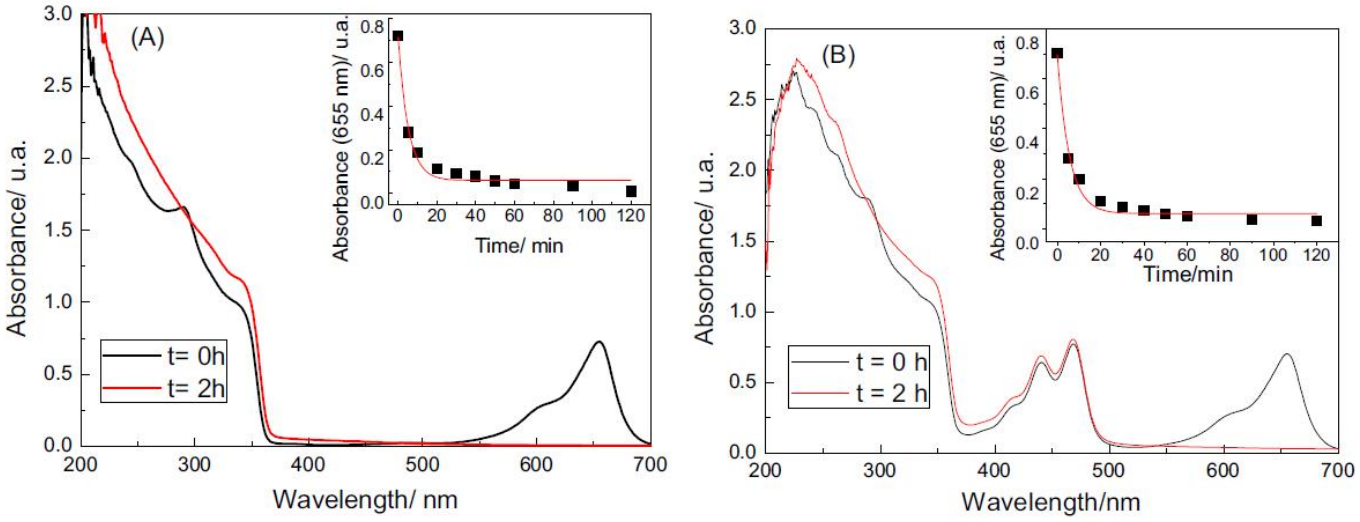

Fig. 9. (A) UV–vis spectra and determination of MB photocatalysis rate constants in ethanol under sunlight irradiation with (A) pure ZnO QDS and (B) ZnO + PerLC QDs. The concentration of PerLC was 2.0×10^{-5} mol L^{-1} and the concentration of ZnO was $2{,}0 \times 10^{-3}$ mol L^{-1}.

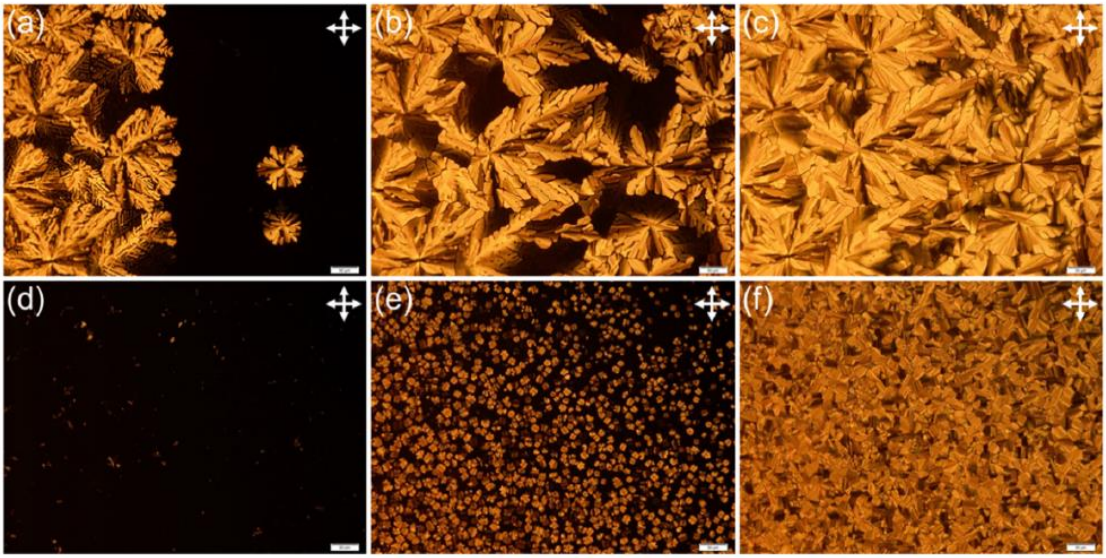

Fig. 10. POM images of pure PerLC (top) and 5.3 wt% doped with ZnO QDs (bottom) during cooling from the isotropic phase and captured at 155 °C (a, d), 140 °C (b, e) and 25 °C (c, f). Images were captured with the sample confined between two glass slides and placed between crossed polarizers. The magnification of the images is 100×. The scale bar corresponds to 50 μm.

4. Conclusion

ZnO quantum dots were successfully synthesized in the presence of a perylene liquid crystal derivative, where the nanoparticle growth was not impeded by the organic molecules. This procedure improved the stability of the colloidal dispersion, which can be associated to the strong coupling between nanoparticles and molecules. Absorption titration experiments allowed the determination of a selective 2:1 stoichiometric ratio between liquid crystal molecules and ZnO nanoparticles. Theoretical simulations underpinned this result by showing a rather strong absorptive interaction with one of the crystallographic planes. The mixture was shown to be an efficient and selective catalyst for methylene blue photodegradation. The ZnO nanoparticles were also homogeneously dispersed into the liquid crystalline matrix, affecting the macroscopic domain size but keeping the columnar liquid crystal mesophase stable over a wide temperature range including room temperature. For practical applications, the observation that the ZnO quantum dots can be efficiently dispersed inside the liquid crystal matrix, together with the stability of both under sunlight irradiation, suggest that the combined system could be applied as n-type semiconducting wide absorbing active layer for photovoltaic applications.

CRediT authorship contribution statement

Wallison C. Costa: Formal analysis, Investigation. **Crislaine Sandri:** Formal analysis. **Samara de Quadros:** Formal analysis, Investigation. **Ana L.E.P. Silva:** Investigation. **Juliana Eccher:** Investigation, Project administration. **Lizandra M. Zimmermann:** Supervision, Project administration, Writing - original draft. **Jose R. Mora:** Formal analysis. **Harald Bock:** Formal analysis, Writing - review & editing. **Ivan H. Bechtold:** Supervision, Project administration, Writing - original draft.

Declaration of competing interest

No conflict of interest.

Acknowledgments

The authors are grateful to CNPq, CAPES, FAPESC-ACAFE, INCT-INEO, H2020-MSCA-RISE-2017 (OCTA, #778158) and CAPES-COFECUB (# 803-14) for financial support, and to LCME-UFSC for TEM facilities.

References

[1] A.A. Mosquera, D. Horwat, A. Rashkovskiy, A. Kovalev, P. Miska, D. Wainstein, J.M. Albella, J.L. Endrino, Sci. Rep. 3 (2013) 1714, https://doi.org/10.1038/srep01714.
[2] Microscopia Eletrônica De Transmissão (Met), https://www.cetene.gov.br/pdf/met.pdf. (Accessed 30 April 2019).
[3] S. Das, C.K. Ghosh, R. Dey, M. Pal, RSC Adv. 6 (2016) 236–244, https://doi.org/10.1039/C5RA20764A.
[4] Ü. Özgür, Y.I. Alivov, C. Liu, A. Teke, M.A. Reshchikov, S. Doğan, V. Avrutin, S.-J. Cho, H. Morkoç, J. Appl. Phys. 98 (2005), 041301. https://doi.org/10.1063/1.1992666.
[5] V.A. Fonoberov, A.A. Balandin, Appl. Phys. Lett. 85 (2004) 5971–5973, https://doi.org/10.1063/1.1835992.
[6] Ü. Özgür, H. Morkoç, Zinc Oxide: Fundamentals, Materials and Device Technology, 1 ed., 2009 490.
[7] J.M. Pietryga, Y.-S. Park, J. Lim, A.F. Fidler, W.K. Bae, S. Brovelli, V.I. Klimov, Chem. Rev. 116 (2016) 10513–10622, https://doi.org/10.1021/acs.chemrev.6b00169.
[8] R. Hardman, Environ. Health Perspect. 114 (2006) 165–172, https://doi.org/10.1289/ehp.8284.
[9] H.Y. Kim, et al., Adv. Funct. Mater. 26 (2016) 3454–3461, https://doi.org/10.1002/adfm.201505549.
[10] Q. Qiao, B.H. Li, C.X. Shan, J.S. Liu, J. Yu, X.H. Xie, Z.Z. Zhang, T.B. Ji, Y. Jia, D.Z. Shen, Mater. Lett. 74 (2012) 104–106, https://doi.org/10.1016/j.matlet.2012.01.048.
[11] G. Bhanjana, N. Dilbaghi, R. Kumar, S. Kumar, Electrochim. Acta 178 (2015) 361–367, https://doi.org/10.1016/j.electacta.2015.07.113.
[12] J.A. Rather, S. Pilehvar, K. De Wael, Sensors Actuators B Chem. 190 (2014) 612–620, https://doi.org/10.1016/j.snb.2013.09.018.
[13] R. Wahab, et al., RSC Adv. 6 (2016) 26111–26120, https://doi.org/10.1039/C5RA25668B.
[14] S.-h. Hsu, Y.Y. Lin, S. Huang, K.W. Lem, D.H. Nguyen, D.S. Lee, Nanotechnology 24 (2013), 475102. https://doi.org/10.1088/0957-4484/24/47/475102.
[15] R. Wahab, S.K. Tripathy, H.-S. Shin, M. Mohapatra, J. Musarrat, A.A. Al-Khedhairy, N. Kumar Kaushik, Chem. Eng. J. 226 (2013) 154–160, https://doi.org/10.1016/j.cej.2013.02.128.
[16] L. Zhang, L. Yin, C. Wang, N. Lun, Y. Qi, ACS Appl. Mater. Interfaces 2 (2010) 1769–1773, https://doi.org/10.1021/am100274d.
[17] S.K. Mandal, et al., Mater. Chem. Phys. 223 (2019) 456–465, https://doi.org/10.1016/j.matchemphys.2018.11.002.
[18] H.-Y. Zhu, L. Xiao, R. Jiang, G.-M. Zeng, L. Liu, Chem. Eng. J. 172 (2011) 746–753, https://doi.org/10.1016/j.cej.2011.06.053.
[19] T. Xu, J. Hu, Y. Yang, W. Que, X. Yin, H. Wu, L. Chen, J. Alloys Compd. 734 (2018) 196–203, https://doi.org/10.1016/j.jallcom.2017.10.275.
[20] S. Muthulingam, I.-H. Lee, P. Uthirakumar, J. Colloid Interface Sci. 455 (2015) 101–109, https://doi.org/10.1016/j.jcis.2015.05.046.
[21] A.K. Srivastava, W. Zhang, J. Schneider, A.L. Rogach, V.G. Chigrinov, H.-S. Kwok, Adv. Mater. 29 (2017), 1701091. https://doi.org/10.1002/adma.201701091.

[22] R.K. Gupta, D. Das, M. Gupta, S.K. Pal, P.K. Iyer, A.S. Achalkumar, J. Mater. Chem. C 5 (2017) 1767–1781, https://doi.org/10.1039/C6TC04166C.
[23] J. Vollbrecht, P. Oechsle, A. Stepen, F. Hoffmann, J. Paradies, T. Meyers, U. Hilleringmann, J. Schmidtke, H. Kitzerow, Org. Electron. 61 (2018) 266–275, https://doi.org/10.1016/j.orgel.2018.06.002.
[24] G. Zhang, K. Zhang, Q. Yin, X.-F. Jiang, Z. Wang, J. Xin, W. Ma, H. Yan, F. Huang, Y. Cao, J. Am. Chem. Soc. 139 (2017) 2387–2395, https://doi.org/10.1021/jacs.6b11991.
[25] A. Gowda, S. Kumar, Materials 11 (2018) 382.
[26] S. Kumar, H.K. Bisoyi, Angew. Chem. Int. Ed. 46 (2007) 1501–1503, https://doi.org/10.1002/anie.200603967.
[27] D.P. Singh, R. Visvanathan, A.E. Duncan, B. Duponchel, Y. Boussoualem, S. Kumar, N.A. Clark, J.F. Blach, R. Douali, A. Daoudi, Liq. Cryst. 46 (2019) 376–385, https://doi.org/10.1080/02678292.2018.1502371.
[28] M. Ozaki, M. Yoneya, Y. Shimizu, A. Fujii, Liq. Cryst. 45 (2018) 2376–2389, https://doi.org/10.1080/02678292.2018.1530375.
[29] M. Zhang, F. Zhang, Q. An, Q. Sun, W. Wang, X. Ma, J. Zhang, W. Tang, J. Mater. Chem. A 5 (2017) 3589–3598, https://doi.org/10.1039/C7TA00211D.
[30] F. Würthner, C.R. Saha-Möller, B. Fimmel, S. Ogi, P. Leowanawat, D. Schmidt, Chem. Rev. 116 (2016) 962–1052, https://doi.org/10.1021/acs.chemrev.5b00188.
[31] J. Eccher, A.C.B. Almeida, T. Cazati, H. von Seggern, H. Bock, I.H. Bechtold, J. Lumin. 180 (2016) 31–37, https://doi.org/10.1016/j.jlumin.2016.08.012.
[32] M.F. Prodanov, et al., Langmuir 29 (2013) 9301–9309, https://doi.org/10.1021/la401475b.
[33] J. Kelber, M.-F. Achard, B. Garreau-de Bonneval, H. Bock, Chem. Eur. J. 17 (2011) 8145–8155, https://doi.org/10.1002/chem.201100939.
[34] L.M. Zimmermann, P.V. Baldissera, I.H. Bechtold, Mater. Res. Express 3 (2016), 075018. https://doi.org/10.1088/2053-1591/3/7/075018.
[35] A. Schejn, M. Frégnaux, J.-M. Commenge, L. Balan, L. Falk, R. Schneider, Nanotechnology 25 (2014), 145606. https://doi.org/10.1088/0957-4484/25/14/145606.
[36] A. Asok, M.N. Gandhi, A.R. Kulkarni, Nanoscale 4 (2012) 4943–4946, https://doi.org/10.1039/C2NR31044A.
[37] P.J. Reid, B. Fujimoto, D.R. Gamelin, J. Chem. Educ. 91 (2014) 280–282, https://doi.org/10.1021/ed300693d.
[38] P.K. Santra, S. Mukherjee, D.D. Sarma, J. Phys. Chem. C 114 (2010) 22113–22118, https://doi.org/10.1021/jp108613f.
[39] X. Liu, X. Xing, Y. Li, N. Chen, I. Djerdj, Y. Wang, New J. Chem. 39 (2015) 2881–2888, https://doi.org/10.1039/C5NJ00070J.
[40] V.A. Fonoberov, K.A. Alim, A.A. Balandin, F. Xiu, J. Liu, Phys. Rev. B 73 (2006), 165317. https://doi.org/10.1103/PhysRevB.73.165317.
[41] X. Ma, Y. Zhao, Chem. Rev. 115 (2015) 7794–7839, https://doi.org/10.1021/cr500392w.
[42] K. Hirose, J. Incl. Phenom. Macrocycl. Chem. 39 (2001) 193–209, https://doi.org/10.1023/a:1011117412693.
[43] A. Beltrán-Porter, D. Beltrán-Porter, A. Cervilla, J.A. Ramirez, Talanta 30 (1983) 124–126, https://doi.org/10.1016/0039-9140(83)80031-9.
[44] A. Calzolari, M.B. Nardelli, Sci. Rep. 3 (2013) 2999, https://doi.org/10.1038/srep02999.
[45] D. Vanderbilt, Phys. Rev. B 41 (1990) 7892–7895, https://doi.org/10.1103/PhysRevB.41.7892.
[46] R. Dovesi, et al., Wiley Interdisc. Rev. Comput. Mol. Sci. 8 (2018) e 1360, https://doi.org/10.1002/wcms.1360.
[47] R. S. Dovesi, V.R.; Roetti, C.; Orlando, R.; Zicovich-Wilson, C. M.; Pascale, F.; Civalleri, B.; Doll, K.; Harrison, N. M.; Bush, I. J.; D'Arco, P.; Llunell, M.; Causà, M.; Noël, Y.; Maschio, L.; Erba, A.; Rerat, M.; Casassa, S. (2017).
[48] Y. Chen, H. Zhao, B. Liu, H. Yang, Appl. Catal. B Environ. 163 (2015) 189–197, https://doi.org/10.1016/j.apcatb.2014.07.044.
[49] E. Muchuweni, T.S. Sathiaraj, H. Nyakotyo, Heliyon 3 (2017), e00285. https://doi.org/10.1016/j.heliyon.2017.e00285.
[50] M.J. Frisch, et al., Gaussian 16 Rev. C.01, 2016 (Wallingford, CT).
[51] R. Steudel, Y. Steudel, Chem. Eur. J. 12 (2006) 8589–8602, https://doi.org/10.1002/chem.200600700.
[52] V.L. Chandraboss; B. Karthikeyan, S. Senthilvelan, Phys. Chem. Chem. Phys. 16 (2014) 23461–23475, https://doi.org/10.1039/C4CP03274H.